Redox Biology 41 (2021) 101911

Contents lists available at ScienceDirect

Redox Biology

journal homepage: www.elsevier.com/locate/redox

Kaempferol alleviates LD-mitochondrial damage by promoting autophagy: Implications in Parkinson's disease

Xiaojuan Han [a,c,d,1,*], Shengnan Zhao [b], Hua Song [b], Tianshu Xu [a,1], Qijun Fang [a], Gang Hu [c,**], Linyun Sun [b,d,***]

[a] Department of Rheumatology and Immunology, Department of Traditional Chinese Medicine, Nanjing Drum Tower Hospital Clinical College of Traditional Chinese and Western Medicine, Nanjing University of Chinese Medicine, Nanjing, China
[b] Department of Rheumatology and Immunology, Nanjing Drum Tower Hospital Clinical College of Nanjing Medical University, Nanjing, China
[c] Department of Pharmacology, Nanjing University of Chinese Medicine, Nanjing, China
[d] Department of Rheumatology and Immunology, Nanjing Drum Tower Hospital, The Affiliated Hospital of Nanjing University Medical School, Nanjing, China

ARTICLE INFO

Keywords:
Kaempferol
Dopaminergic neuron
LDs
Peroxidation
Lipophagy
Parkinson's disease

ABSTRACT

Emerging evidence indicates that unexpected lipid droplet (LD) deposition and peroxidation can accelerate organelle stress and plays a crucial role in the pathogenesis of neurodegenerative diseases (NDDs). In our previous study, we confirmed that kaempferol (Ka), a natural flavonoid small molecule, exhibited neuroprotective effects on mice with LPS-induced Parkinson's disease (PD). In addition, previous studies have shown that autophagy plays an important role in the regulation of cellular LD deposition. In the current study, we showed that Ka protected against TH^+ neuronal loss and behavioral deficits in MPTP/p-induced PD mice, accompanied by reduced lipid oxidative stress in the substantia nigra pars compacta (SNpc). In cultured neuronal cells, Ka exhibited a relatively safe concentration range and significantly suppressed LD accumulation and cellular apoptosis induced by MPP^+. Further study indicated that the protective effect of Ka was dependent on autophagy, specifically lipophagy. Critically, Ka promoted autophagy to mediate LD degradation in lysosomes, which then alleviated lipid deposition and peroxidation and the resulting mitochondrial damage, consequently reducing neuronal death. Furthermore, AAV-shAtg5-mediated Atg5 knockdown abolished the neuroprotective effects of Ka against lipid oxidation in PD mice. This work demonstrates that Ka prevents dopaminergic neuronal degeneration in PD via the inhibition of lipid peroxidation-mediated mitochondrial damage by promoting lipophagy and provides a potential novel therapeutic strategy for PD and related NDDs.

1. Introduction

Parkinson's disease (PD) is a common neurodegenerative disease (NDD) that is pathologically characterized by the progressive loss of dopaminergic (DA) neurons in the substantia nigra pars compacta (SNpc) [1]. Although the exact etiology and natural course of this disease have yet to be fully clarified, numerous system-level processes and dysfunctions, including mitochondrial functions, dopamine homeostasis, neuroinflammation, and autophagy, have been implicated in the pathogenesis of PD [1,2]. Recent reports revealed that lipid droplet (LD)-related lipotoxicity might participate in PD pathology [3,4]. LDs are highly dynamic organelles that emerge from the endoplasmic reticulum (ER) membrane and normally serve as intracellular sites of neutral lipid storage [5]. LDs were recently shown to play a much broader role than fatty acid (FA) storage and participate in many diseases. For example, myeloid cells, including macrophages, leukocytes, and eosinophils, form LDs in response to inflammation and stress, and LDs are sites of inflammatory cytokine production and storage and are

** Corresponding author. Department of Pharmacology, Nanjing University of Chinese Medicine, Nanjing, China.
*** Corresponding author. Department of Rheumatology and Immunology, Nanjing Drum Tower Hospital Clinical College of Nanjing Medical University, Nanjing, China.
* Corresponding author. Department of Rheumatology and Immunology, Department of Traditional Chinese Medicine, Nanjing Drum Tower Hospital Clinical College of Traditional Chinese and Western Medicine, Nanjing University of Chinese Medicine, Nanjing, China.
E-mail addresses: hxj-719@163.com (X. Han), ghu@njmu.edu.cn (G. Hu), lingyunsun@nju.edu.cn (L. Sun).
[1] These authors contributed equally to this work.

https://doi.org/10.1016/j.redox.2021.101911
Received 23 November 2020; Received in revised form 1 February 2021; Accepted 18 February 2021
Available online 3 March 2021

further involved in antigen presentation and pathogen clearance [6]. Importantly, in atherosclerosis, LD-rich foam cells have been demonstrated to be deleterious in all stages of the disease [7].

However, LDs have not been extensively studied in the central nervous system (CNS), with few papers reporting the histological presence of LDs in human brain tissue [8,9]. Even so, LDs may have important functions in the brain, as recent studies confirmed that aggregated LDs in glia accelerated neurodegeneration in a Drosophila model [10]. It has recently been reported that in mice, oil red O-positive lipid-laden cells, including neurons, glial fibrillary acidic portein $(GFAP)^+$ astrocytes and ionized calcium bindingadaptor molecule-1 $(IBA\text{-}1)^+$ microglia, are present in many brain regions and have been shown to participate in age-associated processes [11]. Our previous work also demonstrated increased LD accumulation in the brain in a PD mouse model [12]. Taken together, these studies suggest that LDs may be involved in the pathogenesis of PD, as well as other NDDs.

Normally, intracellular LDs are degraded in lysosomes and deliver FAs to mitochondria for their consumption as an alternative energy source during periods of nutrient depletion [13]. However, neurons have a low capacity for mitochondrial FA consumption for energy production [14]. This characteristic makes neurons particularly sensitive to LD accumulation and peroxidation. Furthermore, the accumulation of LDs enhances the FA oxidation rate and imposes persistent pressure on the mitochondrial electron transport chain, which increases reactive oxygen species (ROS) production by electron transport chain complexes I and III [15] to amplify oxidative stress. Lipid overload also leads to ROS production by extramitochondrial sources such as nicotinamide adenine dinucleotide phosphate (NADPH) oxidases and other oxidative enzymes. Combined with the decreased expression of antioxidant enzymes and the low capacity for FA consumption in neurons, LD accumulation mediates oxidative stress and can further lead to mitochondrial damage, lysosomal dysfunction, defective autophagy, and the activation of inflammatory responses [16,17]. Unless the accumulated LDs can be inhibited or removed, highly active neurons undergo pathophysiology, giving rise to neurodegeneration [17]. Evidence indicates that the lysosome-mediated catabolic process called autophagy plays a pivotal role in maintaining cellular LD homeostasis in multiple tissues [17,18]. In detail, LDs can be selectively sequestered in autophagosomes and delivered to lysosomes for degradation by lysosomal acid lipases, a process specifically known as lipophagy [19]. Therefore, targeting LDs and their autophagic removal pathway could represent a novel approach to managing neurodegeneration.

The study of natural products and dietary agents as sources for potential NDD treatments and strategies has gained enormous interest in recent years [20]. Kaempferol (Ka) is a natural polyphenolic small molecule that can be found in a number of Chinese medicinal herbs and dietary sources [21]. Ka has been reported to exert antibacterial, anti-aging and immunomodulatory effects, as well as antioxidant and neuroprotective activities [20,22,23]. Previously, Ka was reported to inhibit inflammation in BV2 microglial cells in vitro [24] and increase the resistance of DA neurons to neuroinflammation in vivo [25]. However, the effect of Ka on LDs in PD has not yet been investigated.

Given the importance of LDs and the intimate connection between LDs, mitochondria, and autophagy [16], which are all involved in PD, we hypothesize that Ka inhibits LD peroxidation and prevents DA neurodegeneration in PD. In the present study, we demonstrated that Ka significantly protected against neurodegeneration in a murine PD model by inhibiting LD accumulation. Further study revealed that Ka triggered autophagy and reduced the accumulation of oxidized LDs to alleviate mitochondrial dysfunction and mitochondrial ROS (mtROS) production, thereby preventing neuronal apoptotic death. The findings obtained in this study may help direct clinical decisions regarding the use of the natural molecule Ka in NDDs such as PD.

2. Materials and methods

2.1. Experimental animals

C57BL/6J mice (male, 4-month old) were obtained from Nanjing Medical University Animal Core (Nanjing). Mice were maintained and bred in the Animal Resource Centre of the Faculty of Medicine, Nanjing Medical University and in the animal facility at Nanjing Drum Tower Hospital. Mice are free to access to food and water in a room with an ambient temperature of 22 °C ± 2 °C and a light/dark cycle of 12:12 h. All animal procedures were carried out in strict accordance with the guideline of the National Institutes of Health Guide for the Care and Use of Laboratory Animals.

2.2. Reagents

MPTP (M0896), 3-MA (M9281), penicillin-streptomycin (V900929), sodium pentobarbital and probenecid were purchased from Sigma-Aldrich (St. Louis, MO, USA). Kaempferol (HPLC > 95%) for in vivo treatment was purchased from Nanjing Jingzhu Bio-technology Co., Ltd (Nanjing, China), kaempferol (HPLC > 99.0%, 96,353) for in vitro experiments was obtained from Sigma-Aldrich (St. Louis, MO, USA). BODIPY 493/503 (D3922), BODIPY 581/591 C11 (D3861), DHE (D11347) were purchased from Thermo Fisher Scientific. For animal experiments, Ka was dissolved in a solution of 10% DMSO in 16% SBE-β-CD in sterile saline. For cell experiments, Ka was prepared in DMSO (Sigma-Aldrich) and PBS (final DMSO concentration is 0.01%), pH 7.4.

2.3. Induction and treatment of methyl-4-phenyl-1,2,3,6-tetrahydropyridine (MPTP)- induced PD mouse model

To evaluate the effects of Ka in the PD model of MPTP/p-toxicity, mice (male, aged 4–5 months old) were randomly divided into saline-treated group, MPTP-treated group, MPTP + Ka-treated group, and Ka alone treated group. In the MPTP-treated group, mice received chronic MPTP administration with protocol similar to that described previously [26]: MPTP was dissolved in saline and injected subcutaneously at 25 mg/kg followed by 250 mg/kg probenecid (dissolved in dimethyl sulfoxide) intraperitoneally (i.p.) injection at intervals of 1 h every 3.5 days over a period of 5 weeks. Control mice received saline and probenecid injection. In the MPTP + Ka-treated group, mice received Ka (50 mg/kg, a single injection/day during experiments, Jingzhu Biotechnology, Nanjing, China) intraperitoneally (i.p.) daily 3 d prior to treatment with MPTP and over the 5 MPTP injection weeks. One week after the last MPTP injection, mice were subjected to behavioral testing blinded to groups. After, all mice were anesthetized with 40 mg/kg sodium pentobarbital and sacrificed for brain proteins detection and immunohistochemistry or qPCR analysis.

2.4. In vivo stereotaxic surgery and experimental treatments

Stereotaxic surgery under sodium pentobarbital anesthesia (40 mg/kg, i.p.) was performed as described [25]. Mouse *Atg5* and control shRNA was transfected with packaging vectors (AAV-U6-CMV-shRNA-EGFP) to generate AAV. For microinjection, anesthetized mice are placed in a stereotaxic apparatus. They were injected with the 1 μL AAV by glass electrode aiming at DG (AP: − 0.3 mm; ML: ± 0.13 mm; DV: − 0.45 mm) at a rate of 0.25 μL/min. Then the needle was retained for additional 2-min. 2 weeks after virus microinjection, mice were subjected to MPTP-induced PD model conduction and (or) Ka treatment.

Atg5 shRNA was obtained from Hanbio Biotechnology (Shanghai, China) Co., Ltd. For the Atg5 silence, the primers were shown in Supplementary Table 1.

2.5. Behavioral analysis

One week after the final injection of MPTP or saline, the rotarod test and pole test were performed as described before [27]. For the rotarod test, mice were acclimatized to the rotarod in two trials (6 min with an accelerated speed of 12–20 rpm) per day for 2 consecutive days before the start of the experiment. Then, the mice were tested at 20 rpm for 300 s for other 3 consecutive days. The latency to fall was recorded using Rotarod Analysis System (Jiliang, Shanghai, China). For the pole test, mice were placed head up on the top of a vertical wooden pole (rough-surfaced, height 50 cm, diameter 1 cm). All mice were accustomed to the apparatus 2 days before testing and then tested for three times in the third day. The total time (T-total, until the mouse reached the floor with its four paws) and the turn time (T-turn, for the mouse to turn completely head downward) were recorded. The experiment was blinded to mouse groups for each behavioral testing and the test was performed three times.

2.6. Brain sample collection

After the final behavioral tests, mice were anesthetized by sodium pentobarbital (40 mg/kg, i.p.). For q-PCR, western blotting and high-performance liquid chromatography (HPLC) analysis, the whole brains were rapidly extracted from animals then the midbrain and stratum tissues were quickly dissected, pre-frozen by liquid nitrogen. All samples were stored at −80 °C until analysis.

For immunohistochemical analysis, mice were perfused transcardially with 4% paraformaldehyde (PFA). Brains were extracted, post-fixed, dehydrated, embedded in OCT (Tissue-Tek), and serial sections of the brains were cryosectioned (30 μm per slicen) through each entire stratum and midbrain using a freezing microtome (Leica CM1950, Nussloch, Germany). All sections were collected in six separate series and brain slices were stored in 50% glycerin and frozen in −20 °C until analysis.

For TEM, mice were perfused with 2.5% glutaraldehyde and 2% paraformaldehyde as described [12]. A small portion (<1 mm^3) of the mesencephalon was carefully sectioned and incubated in the same fixative for 2 h at 4 °C. Specimens were postfixed in 1% osmium tetroxide, stained in aqueous uranyl acetate, and then dehydrated and embedded in epoxy resin. Ultrathin sections were stained using lead citrate and examined with transmission electron microscope (JEM-1010, Tokyo, Japan).

2.6. Immunohistochemical analysis

Brain slices were rinsed in PBS followed by 3% H_2O_2 for 10 min then incubated with 0.3% Triton X-100 in PBS supplemented 5% BSA for 1 h. After that, slides were incubated with the primary antibodies at 4 °C overnight in PBS containing 5% BSA at 4 °C overnight, then washed and incubated in secondary antibodies for 1 h at room temperature, followed by incubating with diaminobenzidin (DAB) or mounting in DAPI (Life Technologies, Cat P36931) as immunofluorescent staining for 5 min. For Nissl staining, the slides were merged in cresyl violet (CV) solution (0.1 g cresyl violet, 99 ml H_2O and 1% acetic acid 1 ml) for 30 min at room temperature then dehydrated with alcohol and xylene. Images were observed and photographs were captured under an Olympus BX52 microscope (Olympus America Inc., Melville, NY, United States). The total number of TH-positive and Nissl's-positive neurons in the SNpc was obtained stereologically by using the optical fractionator method with MicroBrightField Stereo-Investigator software (MicroBrightField, Williston, VT, USA).

2.7. High-performance liquid chromatography (HPLC) analysis

Mice striatal samples were homogenized with 0.1 M perchloric acid (1 mg tissues in 100 μL perchloric acid) and 0.1 mM EDTA, treated by ultrasonic and centrifuged at 20,000 rpm for 30 min as reported [27]. Then supernatant liquids were collected for measuring. The mobile phase is a mixed solution consisting of 90 mM sodium phosphate monobasic, 1.7 mM 1-octanesulfonic acid, 50 mM citrate, 50 μM EDTA, 10% acetonitrile with the flow rate of 0.2 ml/min. In parallel, for quantitative standard curve calculation, stock standards solution for dopamine and dihydroxy-phenyl aceticacid (DOPAC) (Sigma-Aldrich, USA) were prepared in 0.1 M $HClO_4$. Amount of 10 μl of prepared supernatant or standard solution was injected into the mobile phase and tested by ESA Coulochem III electrochemical detector (Coulochem III, Thermo Fisher Scientific). Samples were measured and peaks were quantified. The concentrations of monoamines were quantified by comparing with the standard using ClarityChrom software (Knauer, Germany) and then the contents in stratum were converted according to the dilution ratio. The standard curve of DA and DOPAC were shown in Supplementary Fig. 1a and b.

2.8. Cells cultures and treatments

Mesencephalic primary neuron cultures were conducted as described previously [12]. In brief, the mesencephalic tissues of C57BL/6 mice on embryonic day 14/15 (E14/15) was carefully removed, mechanically dissociated to remove the membranes and large blood vessels and then dissected. Next, they were digested with trypsin-EDTA (Amresco, Solon, OH, USA) and then filtered through a 100-μm filter to obtain a single cell suspension. Subsequently, the cells were plated on poly-L-lysine-precoated 12-/24-well plates at 2.5 × 10^5 cells/ml containing Neurobasal medium (Cat 21103049,Gibco™, Thermo Fisher Scientific, Rockford, USA) supplemented with B27 (2% v:v, Cat 17504044,Gibco™) and penicillin/streptomycin (0.5% v:v). The cultures were maintained in a humidified chamber (37 °C, 5% CO2 incubator).The culture medium was changed every 3 days and cells can be used at 7–10 days.

Cell lines: SH-SY5Y cell lines were cultured in 10% FBS and 1% penicillin/streptomycin in a humidified incubator at 37 °C and 5% CO_2. In the experiments, SH-SY5Y cells were treated with MPP^+ (200 μM) or different doses of Ka (0, 3, 30, 60, 100, 300, 600 μM) for 24 h. Ka (3, 10, 30, 60 μM, 3 h) primed–SH–SY5Y cells were stimulated with MPP^+ (400 μM) for 24 h. Ka (30 μM, 3 h) with (or without) 3-MA (3 mM, 1 h) or α-tocopherol (50 μM, 1 h, Sigma-Aldrich, 47783) primed–SH–SH5Y cells were stimulated with MPP^+ (200 μM) for 24 h.

2.9. Cell viability CCK8 assay

The changed cell viability of Ka treatment was detected by Cell Counting Kit-8 (CCK-8 Kit, Selleck, Houston, TX, USA). In brief, SHSY5Y cells were seeded in a 96-well plate and then treated with different concentrations of Ka (3, 30, 60, 100, 300, 600 μM) for 24 h. Then 10 μl of CCK-8 reagent was added to each well for 4 h. Finally, the absorbance was detected by the Multiskan Spectrum (Thermo Fisher Scientific) at 450 nm.

2.10. ATP assay

The cellular ATP levels were detected by an ATP Bioluminescence Assay Kit (Beyotime Biotechnology Co., China) according to the manufacturer's instructions. After treatment, cells were lysed and centrifuged at 12,000 rpm for 5 min at 4 °C and the supernatants were collected. Working solution (100 μL) was added to 20 μL of sample in the 96-well plate, and the luminescence was measured immediately on an automated microplate reader. Measurements from all samples were normalized to protein concentration.

2.11. Na^+-K^+-ATPase assay

For Na^+-K^+-ATPase measurement (A070-2-2, Jiancheng, Nanjing, China), cells were sonicated and centrifuged at 6000 rpm for 10 min to

acquire supernatant. Reaction solutions of Na^+-K^+-ATPase detection were added and incubated according to the manufacturer's instructions. Then the absorbance at 660 nm was detected. Measurements of all samples were normalized to protein concentration.

2.12. Western blotting analysis

Cells or brain tissues were lysed in the RIPA buffer (50 mM Tris (pH 7.4), 150 mM NaCl, 1% NP-40 (FNN0021, Thermo), 0.5% sodium deoxycholate (D6750, Sigma), 0.1% SDS (74255, Sigma) supplemented with protease and phosphatase inhibitors (Roche, Shanghai, China). Protein concentrations were determined with the Micro BCA Kit (Beyotime, Shanghai, China). A 30-μg protein of each sample were separated by SDS–PAGE using polyacrylamide TGX gels (Bio-Rad, Hercules, California, USA) and then transferred to polyvinylidene difluoride (PVDF) membranes (Millipore, Bedford, MA). After blocking, PVDF membranes were incubated with various specific primary antibodies in TBST at 4 °C overnight then washed and incubated in corresponding horseradish peroxidase (HRP) conjugated secondary antibodies for 1 h at room temperature. Immunoreactive bands were visualized and detected by enhanced chemiluminescence (ECL) plus detection reagent (Pierce, Thermo Fisher Scientific, Rockford, IL) and analyzed using the ImageQuant™ LAS 4000 imaging system (GE Healthcare, Pittsburgh, PA, USA).

2.13. Real time quantitative (Q)-and reverse transcription (RT)-PCR

Total RNA was extracted from brain tissues and cultured cells using Trizol reagent (Invitrogen, Carlsbad, CA, USA). Reverse transcription was carried out using TAKARA PrimeScript RT reagent kit (TaKaRa, Japan). Realtime qPCR was carried out using SYBR Green Master Mix (Applied Biosystems) in a StepOnePlus instrument (Applied Biosystems). The primers were purchased and validated from Generay (Shanghai, China). The primers used for qPCR were shown in Supplementary Table 2.

2.14. Lactate dehydrogenase (LDH) assay

According to the manufacturer's instructions, cells were planted in 96-well plate at 5000 cells/well and culture medium was collected to measure LDH levels with an assay kit (Nanjing Jiancheng Bioengineering Institute). Then the absorbance of samples was detected by the Multiskan Spectrum (Thermo Fisher Scientific) at 450 nm.

2.15. BODIPY493/503, BODIPY 581/591 C11 and MitoTracker deep red staining

Live cells were washed with PBS and incubated with 2 μg/ml BODIPY 493/503 (Invitrogen™, Cat D3922) or BODIPY 581/591 C11 (BD-C11) (2.0 μM, Invitrogen™, Cat D3861) in PBS for 15 min at 37 °C. For MitoTracker Deep Red staining, live cells were incubated with 0.5 μg/ml MitoTracker Deep Red (Invitrogen™, Cat M22426) in PBS for 30 min at 37 °C. Then cells were washed twice in PBS and fixed in 3.5% PFA for 10 min followed by washing and counterstaining with Hoechst 33342 (Sigma, Cat B2261) for 10 min before being covered on glass slides for imaging. Images were observed and photographs were captured by fluorescence microscopy (Olympus, Tokyo, Japan).

2.16. Hoechst and PI staining

Cells were stained with Hoechst 33,342 (1 μl diluted in 500 μl PBS, Sigma, Cat B2261) and (or) PI (0.1 μl diluted in 500 μl PBS, Solarbio, CA1020) for 10 min and then fixed and observed by fluorescence microscopy (Olympus, Tokyo, Japan).

2.17. Flow cytometry

Cells were digested and rinsed with D-hank's then stained with Annexin V-FITC (5 μl diluted in 500 μl PBS)/PI (0.1 μl diluted in 500 μl PBS) apoptosis kit (CA1020, Solarbio, Beijing, Chian) according to the manufacturer's protocol. After, apoptotic cells were analyzed using flow cytometry (guava easyCyte™ 8, Millipore, USA). Mitochondrial ROS and mitochondrial membrane potential measurements were performed as published [12]. SH-SY5Y cells were stained with MitoSOX (2.5 μM, Invitrogen, USA) or with JC1 (10 μg/ml, T-3168, Invitrogen, USA) at 37 °C for 30 min. After washing with PBS twice, the cells were then resuspended in cold PBS containing 1% FBS for flow cytometric analyses. Data were analyzed with the FCS Express software (Guava Easy Cyte™8, Millipore, Hayward, CA, USA).

2.18. Seahorse respiration assays

Mitochondrial respiratory function in live SH-SY5Y cells was measured using the Seahorse extracellular flux (XFe96) analyzer (Agilent, Santa Clara, USA) via changes in the oxygen consumption rate (OCR). SH-SY5Y cells seeded at 3×10^3 cells/well were allowed to adhere to the Seahorse cell culture plates and to reach approximately 80% confluency at the time of the experiment. The following day, cells were pretreated with Ka and then exposed to MPP^+ for another 24 h. OCR was detected under basal conditions followed by sequential addition of 1 μM oligomycin, 1 μM FCCP, as well as 1 μM rotenone & antimycin A.

2.19. Statistical analysis

Data were presented as mean ± SEM. The significance of difference was determined by Student's *t*-test, Two-way analysis of variance or one-way analysis of variance (ANOVA) followed by Tukey's post hoc test. Difference was considered significant at $P < 0.05$.

3. Results

Result 1. Ka restores motor dysfunction and increases dopamine levels in the striatum of MPTP/p PD model mice

To investigate the neuroprotective effect of Ka on PD pathogenesis, 4-month-old male C57BL/6 mice were injected with the neurotoxin MPTP to establish the MPTP/p PD model and were treated with Ka (Fig. 1a). After model induction, the rotarod test and the pole test were used to evaluate the motor and behavioral performance of mice in the different groups. As shown, the rotarod performance time was markedly reduced in MPTP-treated mice, and this effect was prevented by Ka (Fig. 1b). Ka also restored the behavioral deficits induced by MPTP, as indicated by the reductions in the turning time and total time in the pole test (Fig. 1c and d), without affecting the body weights of the mice (Fig. 1e). Furthermore, HPLC analysis showed that the level of dopamine in the striatum was significantly decreased in MPTP/p-challenged mice, and this level was restored by Ka treatment (Fig. 1f). Ka treatment also alleviated the MPTP/p-induced reduction in dihydroxy-phenyl acetic acid (DOPAC, a metabolite of dopamine) levels in the striatum (Fig. 1g). These results suggest that Ka restores motor dysfunction and increases dopamine levels in the striatum in MPTP-induced PD mice.

Result 2. Ka alleviates the loss of DA neurons in the SNpc of MPTP/p PD model mice

Next, to further evaluate the neuroprotective effect of Ka on MPTP/p-induced DA neuronal impairment, we examined tyrosine hydroxylase $(TH)^+$ neurons in the murine SNpc by immunostaining. As shown in Fig. 2a and b, MPTP/p induced a significant reduction in the number of TH^+ neurons, which was alleviated by Ka treatment. Furthermore, stereological counts of total neurons in the SNpc, as defined by Nissl

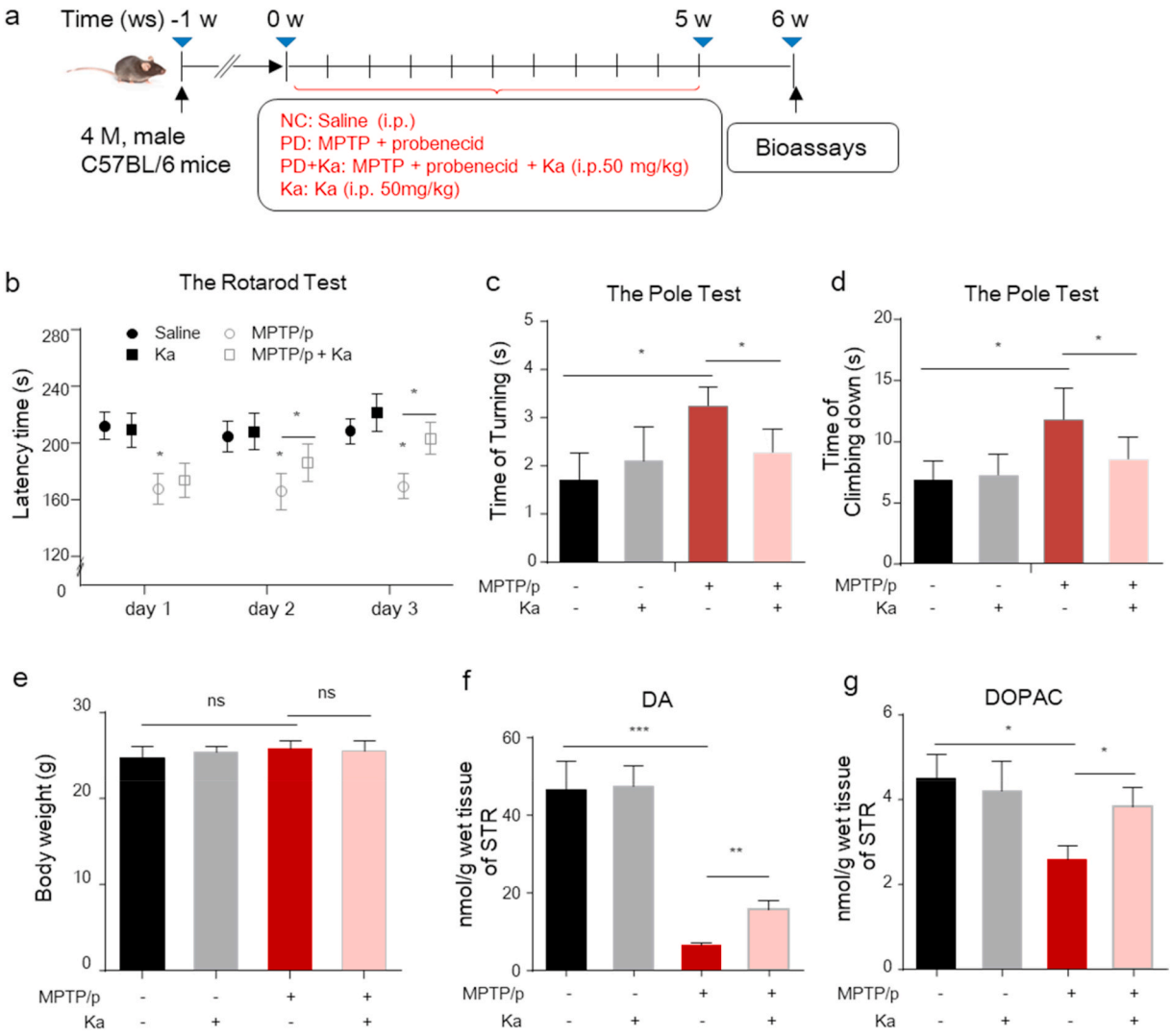

Fig. 1. Ka treatment alleviates motor dysfunction and increases dopamine levels in the striatum of MPTP/p PD model mice.
(a) Schematic diagram of the experimental design.(b) Time on the rod was measured for the rotarod test on three consecutive days. (c–d) The time taken to turn around (time of turning) and descend a pole (time of climbing) were recorded for the pole test. (e) Mouse body weights were measured at the end of the study. (f–g) Dopamine (DA) and dihydroxy-phenyl acetic acid (DOPAC) in the striatum were analyzed by high-performance liquid chromatography. The data are expressed as the mean ± SEM. n = 9–10 for each group in (b, c, d); n = 6–8 for each group in (f, g). ns, not significant, $^{*}P < 0.05$, $^{**}P < 0.01$, $^{***}P < 0.001$, by one-way ANOVA followed by Tukey's post hoc test. MPTP, 1-methyl-4-phenyl-1,2,3,6-tetrahydropyridine; Ka, kaempferol.

staining, verified that the loss of TH^+ cells reflected cellular death but not the downregulation of TH expression and showed that Ka treatment restored the decrease in the number of Nissl-positive neurons in the SNpc of MPTP-treated mice from 43.3% to 25.4% (Fig. 2c and d). In addition, Ka significantly ameliorated the MPTP-induced reduction in TH and DAT protein expression, as measured by Western blotting (Fig. 2e–g). This evidence confirms the neuroprotective effect of Ka on the PD mouse model.

Result 3. Ka reduces the accumulation of LD vacuoles and oxidative stress in the SNpc of MPTP/p-treated mice

Increasing evidence has shown the involvement of LDs in NDDs [10], consistently, our previous work identified increased LDs in the SNpc of MPTP-induced PD mice [12]. LDs can be easily identified and show round, low-density structures with homogenous amorphous contents [28]. Normally, LDs can be degraded via autophagy to avoid accumulation [29]. To investigate whether Ka could regulate LDs in PD, the accumulation of LDs was analyzed by transmission electron microscopy (TEM) in the SNpc of control, MPTP/p, and MPTP/p + Ka mice. As shown in our previous work [12], the number and size of LDs were increased in MPTP/p mice compared to saline-treated controls (Fig. 3a and b) and were significantly reduced in Ka-treated mice (Fig. 3c–e). Moreover, in Ka-treated mice, LDs were more frequently observed nearby to, enclosed in or degraded by autolysosomes, which were defined as electron-dense lipofuscin granules. Further histological staining of TH^+ neurons with BODIPY, a dye that specifically labels neutral lipids and is commonly used to detect LDs [30], showed that both the number and size of $BODIPY^+$ LDs in the SNpc were higher in PD mice than in controls, and were significantly decreased by Ka treatment (Fig. 3f–h).

If LDs cannot be degraded in a timely manner, the accumulated LDs may undergo peroxidation and contribute to mitochondrial ROS-mediated stress [4], which amplifies neurotoxicity and disease progression. Hence, we further examined the expression profiles of genes associated with protection against free FA toxicity (*Gpx8*), neutralizing oxidative species, superoxide radicals (*Sod3*) and hydrogen peroxide (*Cat*), and FA metabolism (*Acsbg1* and *Dbi*) as reported [31], all of which were strikingly decreased in the SNpc of MPTP-treated mice compared with controls, and these effects were ameliorated in Ka-treated PD mice (Fig. 3i). Similarly, MPTP/p also increased the mRNA expression levels

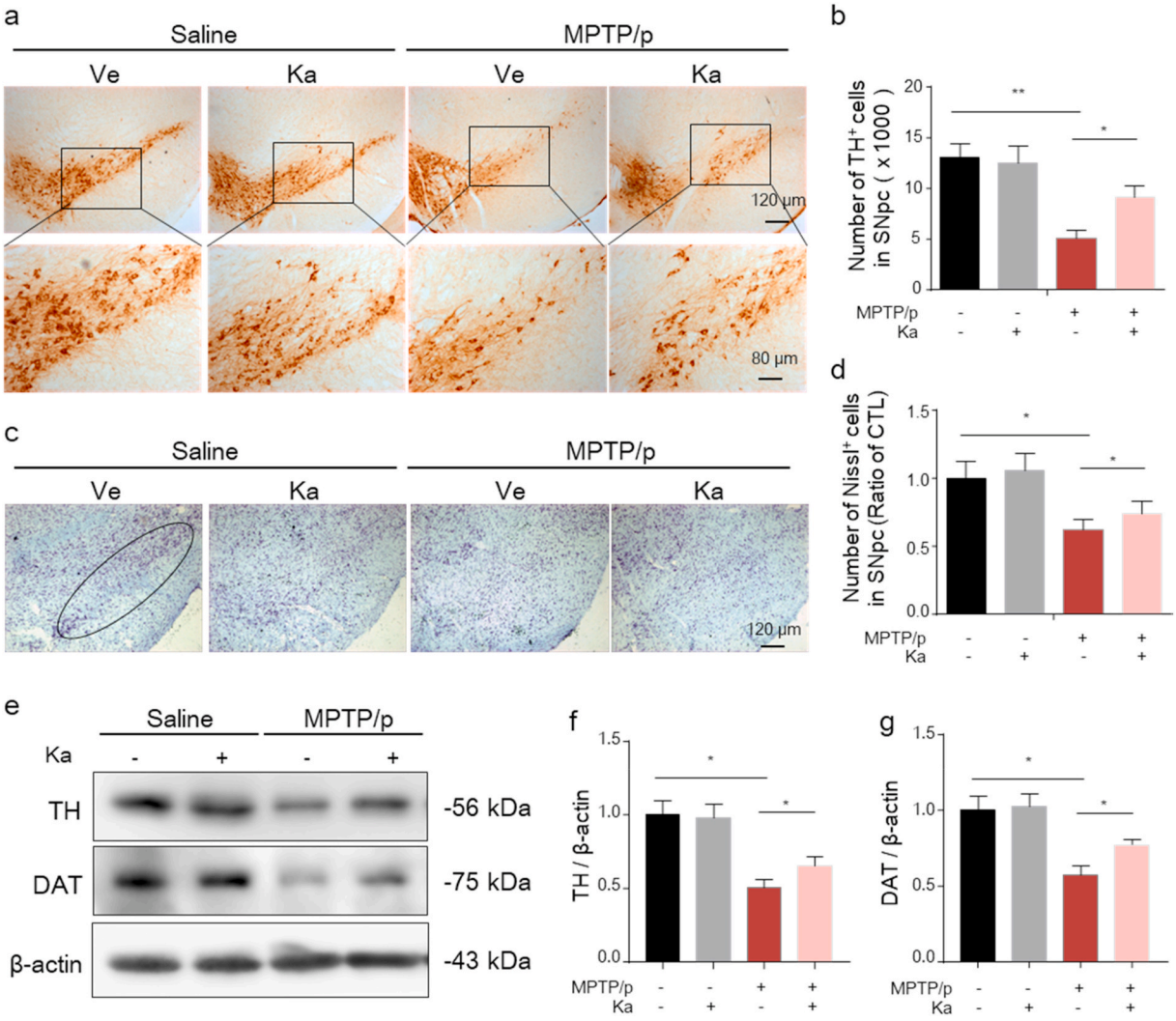

Fig. 2. Ka ameliorates the loss of DA neurons in the SNpc of MPTP/p PD model mice.
(a–b) Microphotographs of tyrosine hydroxylase (TH)-positive neurons (a) and stereological counts of TH-positive neurons in the substantia nigra pars compacta (SNpc) (b). Scale bars are as indicated. (c–d) Microphotographs of cresyl violet-positive cells (c) and stereological counts of cresyl violet-positive cells in the SNpc (d). Scale bar, 120 μm. (e–g) Western blot analysis of TH and DAT protein expression in the SNpc (e) and quantitative analysis (f, g). The quantified data are normalized to the saline control group.The data are expressed as the mean ± SEM. *$P < 0.05$, **$P < 0.01$, by one-way ANOVA followed by Tukey's post hoc test. n = 4–5 for each group. Ve, vehicle, Ka, kaempferol; MPTP, 1-methyl-4-phenyl-1,2,3,6-tetrahydropyridine. . (For interpretation of the references to colour in this figure legend, the reader is referred to the Web version of this article.)

of NADPH oxidase subunits such as *Nox1*, *Nox2*, and *Nox4* in the SNpc of MPTP/p mice, which were further blunted by Ka treatment (Fig. 3j). Taken together, these data suggest that Ka alleviates MPTP/p-induced LD accumulation, peroxidation, and ROS-mediated stress.

Result 4. Ka protects SH-SY5Y cells against MPP^+-induced apoptosis

MPP^+, the active metabolite of MPTP, inhibits mitochondrial complex enzymes and causes the cell death that is directly associated with PD [32]. We next investigated whether Ka could prevent MPP^+-induced neuronal apoptosis in vitro. As shown in Fig. 4a and b, MPP^+ (400 μM, 24 h) induced the release of LDH from SH-SY5Y cells, and Ka (30 and 60 μM) significantly attenuated LDH release without affecting cell survival (Fig. 4a). Since Ka induced a substantial protective effect at a concentration of 30 μM (Fig. 4b), we used this concentration in subsequent experiments. The Hoechst/PI staining results also showed that Ka significantly reduced the percentage of cells with MPP^+-induced chromatin condensation (Fig. 4c and d) and cellular apoptosis, as evidenced by the increased Hoechst fluorescence intensity (Fig. 4c) and the percentage of Hoechst/PI-stained cells ($Hoechst^+/PI^+$) (Fig. 4e). Also, as detected by flow cytometry, MPP^+ induced cell apoptosis, evidenced by the increased percentage of Annexin V-stained cells (AV^+/PI^- and AV^+/PI^+) was protected by Ka (Fig. 4f and g). Additionally, Ka notably reversed MPP^+-induced changes in apoptosis-related protein expression, as evidenced by the upregulation of Bcl-2, downregulation of Bax (Fig. 4hi-j) and reduced cleavage of caspase-3 (Fig. 4h, k). These data suggest that Ka can abolish the detrimental effects of MPP^+ on cell survival.

Result 5. Ka suppresses MPP^+-induced LD accumulation and lipid peroxidation, which mediate mitochondrial damage in SH-SY5Y cells

Recent studies have shown that unexpected LD accumulation can result in increased lipid peroxidation-mediated stress and accelerate mitochondrial dysfunction, which promotes neurodegeneration [10]. Our previous work also showed that the increased LDs in the SNpc were associated with PD pathology in mice [12]. To investigate whether the protective effect of Ka was related to LD accumulation in vitro, we first performed LD-specific staining in SH-SY5Y cells using BODIPY 493/503 and observed increased LD deposition (enhanced levels of neutral lipids)

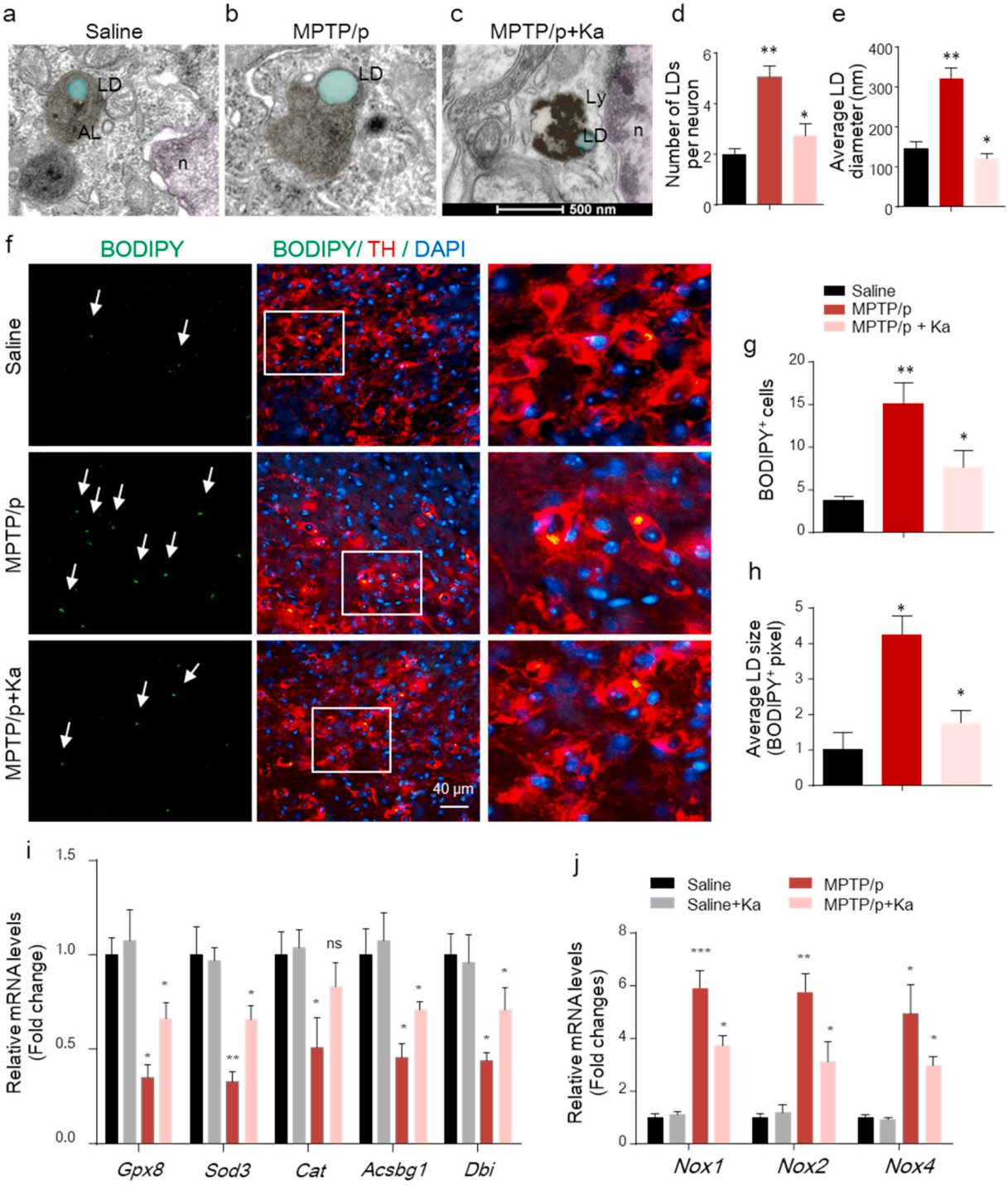

Fig. 3. Ka reduced the accumulation of electron-dense LD vacuoles and lipid oxidation in the SNpc of MPTP/p-treated mice.
(a–c) Representative EM images showing electron-bright vacuoles (lipid droplets), electron-dense autophagic vacuoles containing autolysosomes (ALs), or lipofuscin-containing lysosomes (Lys) in the SNpc of mice treated with saline (a), MPTP/p (b), and MPTP/p + Ka (c). Scale bars, 500 nm. With (a, b) as indicated in our previous work (PMID: 29967574). (d–e) Quantification of electron-bright LD vacuoles per neuron in the SNpc in the indicated mice. n = 3 mice, 10–12 neurons per group. (f–h) Midbrain sections from saline-, MPTP/p-, and MPTP/p + Ka-treated mice were stained for BODIPY (LDs) and TH (DA neurons). The right-most panels show magnifications of BODIPY + TH + neurons. Arrows indicate LDs. (g–h), Quantification of BODIPY$^+$ LD number and size. (i–j) mRNA expression of FFA toxicity-related genes (*Gpx8*, *Sod3*, *Gat*, *Acsbg1* and *Dbi*) (i) and oxidative stress genes (*Nox1*, *Nox2*, and *Nox4*) (j) in the SNpc of the indicated mice was analyzed by real-time qPCR. n = 4–5 per group, three independent experiments.The data are expressed as the mean ± SEM; ns, not significant, $^*P < 0.05$, $^{**}P < 0.01$, $^{***}P < 0.001$, by one-way ANOVA followed by Tukey's post hoc test. Ka, kaempferol; MPTP, 1-methyl-4-phenyl-1,2,3,6-tetrahydropyridine.

in MPP$^+$-treated cells, which was reversed by Ka (Fig. 5a and b). Increased neuronal activity is predicted to trigger lipid and FA peroxidation [33] and can be induced by MPP$^+$ exposure. We then assessed whether the deposited LDs underwent peroxidation following MPP$^+$ treatment using the ratiometric lipid peroxidation sensor BODIPY 581/591 C11 (BD-C11). Following peroxidation, the fluorescence emission peak of BD-C11 shifts from 590 (red) to 510 (green) nm [34]. We observed an increase in the BD-C11 ratio (green-to-red) in SH-SY5Y

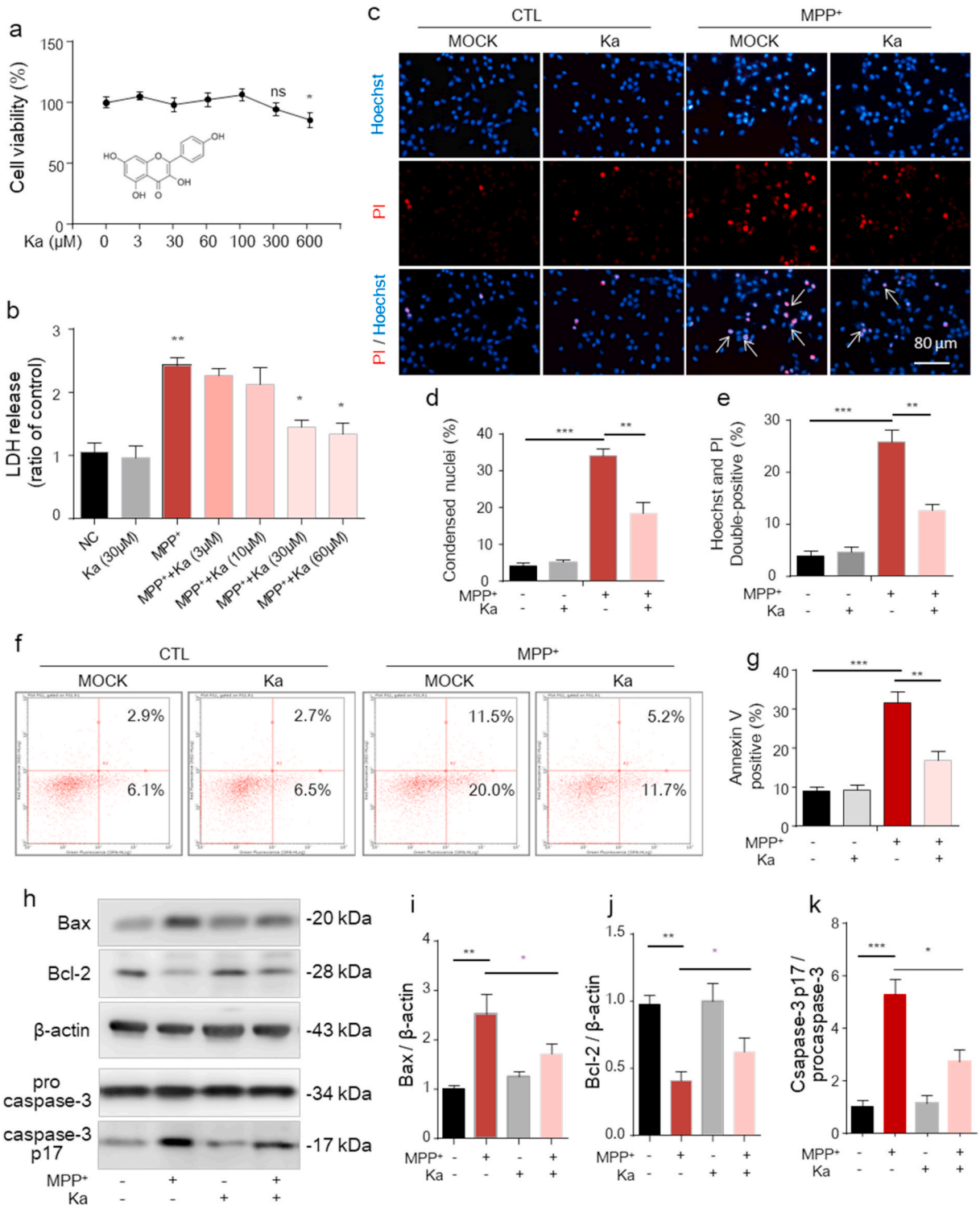

Fig. 4. (a) Cell viability was measured in Ka-treated (0, 3, 30, 60, 100, 300, or 600 μM; 24 h) SH-SY5Y cells by CCK-8 assays. The chemical structure of Ka is shown under the curve. (b) LDH assays of SH-SY 5Y cells treated with Ka (3, 10, 30, or 60 μM) and/or MPP^+ (400 μM, 24 h). (c– e) Ka (30 μM)- and/or MPP^+ (400 μM)-treated SH-SY5Y cells were stained with Hoechst 33,342 and PI and then observed by fluorescence microscopy. Scale bars, 80 μm. Quantification of Hoechst-positive (d) and Hoechst/PI double-positive (e) cells was performed. (f–g) SH-SY5Y cells treated with Ka (30 μM)- and/or MPP^+ (400 μM) for 24 h, then apoptosis was assessed by Annexin V/PI staining and flow cytometry. The data for flow cytometry analysis are presented as a percentage of the cell population by normalizing to control samples. (h–k) Ka (30 μM)-pretreated SH-SY5Y cells were stimulated with or without MPP^+ (400 μM). Representative immunoblots (h) and quantitative analysis of Bcl-2, Bax, procaspase-3 and cleaved caspase-3 in cell extracts (i, j,k). The data are expressed as the mean ± SEM and are representative of at least three independent experiments. $^*P < 0.05$, $^{**}P < 0.01$, $^{***}P < 0.001$, by one-way ANOVA followed by Tukey's post hoc test. Ka, kaempferol.

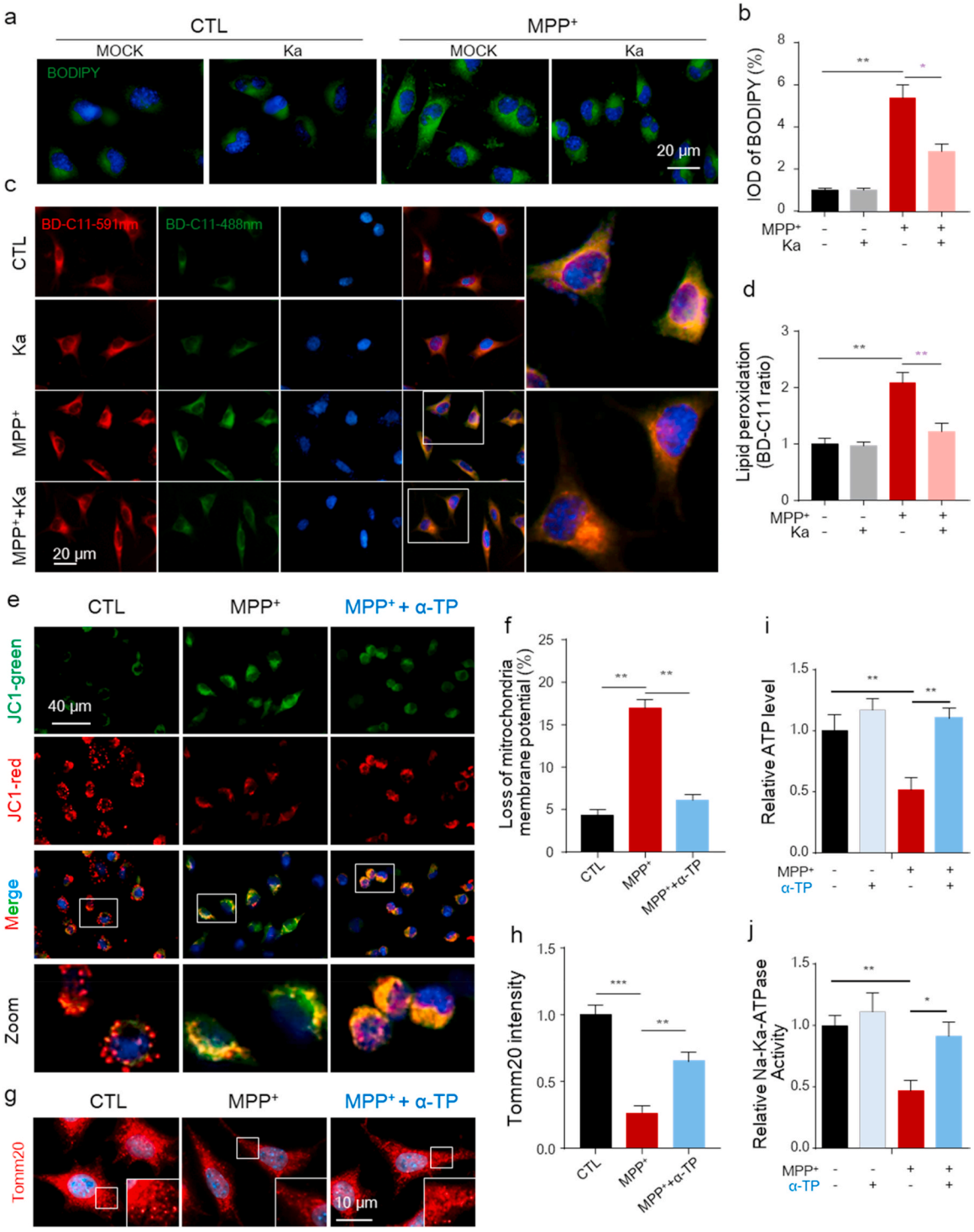

Fig. 5. Ka suppresses MPP^+-induced LD accumulation and lipid oxidation-mediated mitochondrial damage in SH-SY5Y cells.SH-SY5Y cells were pretreated with Ka (30 μM) for 3 h before MPP^+ (400 μM) stimulation for 24 h (a–b) Representative images of BODIPY 493/503 staining (a) and quantitative analysis of LD accumulation (b). The quantified data are normalized to the control group. Scale bars, 20 μm.(c–d) Representative images of BODIPY 581/591 C11 (BD-C11) staining (c). Red (591 nm) and green (488 nm) show total and peroxidized lipids, respectively. Quantitation of the lipid peroxidation ratio (green/red) normalized to the control group (d). Three independent experiments were performed; n = 5 coverslips/treatment. Scale bars, 20 μm. (e–f) Live cells were stained with JC-1 for 30 min and analyzed by microscopy (e). Quantification of the mitochondrial membrane potential (f). Data are representative of three independent experiments, a total number of 18–20 cells/treatment were scored for the quantitative analysis. (g–h) Microscopic analysis of mitochondria was monitored by immunostaining for Tomm20 (g). Quantification of the mitochondrial area normalized to the control group (h). Three independent experiments were performed; 20 cells/treatment were scored for the quantitative analysis.

(i–j) ATP levels (i) and Na^+-K^+-ATPase activity (j) were measured. The data are expressed as the mean ± SEM from three independent experiments. ns, not significant, $^*P < 0.05$, $^{**}P < 0.01$, $^{***}P < 0.001$, by one-way ANOVA followed by Tukey's post hoc test. Ka, kaempferol; MPP^+, 1-methyl-4-phenylpyridinium. . (For interpretation of the references to colour in this figure legend, the reader is referred to the Web version of this article.)

cells treated with MPP^+, indicating increased lipid peroxidation, which was prevented by Ka (Fig. 5c and d).

Alterations in LDs can trigger dysfunction in many intracellular organelles, especially mitochondria [16], and oxidative stress is an important factor involved in mitochondrial damage that can be induced by MPP^+ [35]. Efforts were made to explore the role of lipid peroxidation in MPP^+-induced mitochondrial damage, and we examined changes in mitochondrial potential and mitochondrial morphology in control and MPP^+-treated cells. As observed, there was a decrease in mitochondrial membrane potential in cells treated with MPP^+ (Fig. 5e and f), as well as a reduction in mitochondrial size, as evidenced by immunostaining for Tomm20, a protein located in the outer mitochondrial membrane (Fig. 5g and h), and these effects were alleviated by the addition of a-tocopherol, a specific lipid-soluble antioxidant (Fig. 5e–h). In addition, a-tocopherol significantly alleviated MPP^+-induced energy shortages, as indicated by ATP levels and Na^+-K^+-ATPase activity (Fig. 5i and j), which also reflects mitochondrial function. These data suggest that Ka attenuates MPP^+-induced LD accumulation to prevent lipid peroxidation, which exacerbates mitochondrial damage in SH-SY5Y cells.

Result 6. Ka promotes autophagy and decreases mtROS production in MPP^+-treated SH-SY5Y cells

Normally, LDs are delivered to lysosomes via autophagy and can be broken down into FAs to avoid peroxidation. However, evidence indicates that autophagy is impaired, which plays a crucial role in PD [2]. When autophagy involves portioning LDs to be broken down in lysosomes (Fig. 6a), the process is specifically called lipophagy [2]. To investigate whether autophagy is involved in the neuroprotective effect of Ka, we examined the levels of autophagy-associated proteins. As shown in Fig. 6b–d, in cultured SH-SY5Y cells, the level of microtubule-associated protein light chain 3 (LC3)-II was markedly reduced, while the expression of p62 was markedly increased in MPP^+-treated cells, as measured by immunoblotting, and this effect was significantly reversed by Ka. We further examined the changes in autophagy by immunostaining for LC3. To allow autophagosomes to accumulate within cells, bafilomycin was added to prevent autophagosome fusion with lysosomes. As shown, increased numbers of LC3b puncta were detected in MPP^+-treated cells, indicating impaired autophagic degradation, and this effect was also reversed by Ka (Fig. 6e and f). These results indicate that LDs in SH-SY5Y cells are mobilized by autophagy for eventual removal and that Ka can promote autophagy to reduce oxidized lipid accumulation. Increased lipid peroxidation can exacerbate mitochondrial damage by increasing mitochondrial oxidative stress [4]. Additionally, Ka treatment significantly reduced the robust mtROS generation, as determined by MitoSOX staining (Fig. 6g and h), and decreased the number of dysfunctional mitochondria, as determined by mitochondria-specific labels to distinguish respiring (MitoTracker deep red) and total (MitoTracker green) mitochondria (Fig. 6i and j). In addition, to have a direct view of mitochondrial alterations, we further detected the oxygen consumption rate (OCR) by the Seahorse XF analyzer. As showed in Fig. 6k, the mitochondria respiration were reduced in MPP^+-treated ells, while Ka treatment obviously reverse this damage caused by MPP^+ (Fig. 6k).

Result 7. Autophagy inhibition reverses the suppressive effect of Ka on LD accumulation, mitochondrial dysfunction and DA neuronal injury in vitro

To examine whether autophagy is one of the main mechanisms by which Ka mediates DA neuroprotection, the autophagy inhibitor 3-MA was used. We found that the inhibitory effects of Ka on MPP^+-induced injury, including decreased LD accumulation (Fig. 7a and b), reduced mtROS production (Fig. 7c and d), and alleviated mitochondrial dysfunction (Fig. 7e and f) in SH-SY5Y cells, were significantly blocked by 3-MA. Since LD oxidation and mitochondrial dysfunction are closely associated with DA neuronal death, we next examined primary cultured DA neurons. We treated cultured mesencephalon TH^+ neurons with Ka and/or MPP^+ and quantified the number and length of TH^+ neuronal processes by immunostaining. Morphological analysis revealed that the number and length of neuronal processes were markedly decreased by MPP^+ and protected by Ka, and this protection was further reversed by 3-MA (Fig. 7g–i). These data indicate that Ka alleviates DA neuronal damage by promoting autophagy.

Result 8. Silencing Atg5 abolished the Ka-mediated prevention of neuronal loss in vivo

To further confirm that Ka protects against MPTP/p-induced TH^+ neuronal loss in an autophagy-dependent manner, we silenced *Atg5* by microinjecting an adeno-associated virus (AAV)-expressing a previously characterized shRNA against *Atg5* into the bilateral mesencephalon (Fig. 8a) as previously described [25]. In preliminary experiments, we observed that *Atg5* shRNA transfection for 2 weeks achieved sufficient GFP expression in TH^+ neurons (Fig. 8b) and inhibited ATG5 expression in the SNpc of the injected mice (Fig. 8c). We found that *Atg5*-knockdown reversed the neuroprotective effect of Ka, as evidenced by the upregulated protein expression of TH (Fig. 8d and e) and increased number of TH^+ neurons (Fig. 8f and g). These data further support the contribution of autophagy to the protective effect of Ka in PD mice. In conclusion, we confirmed that Ka protects against MPTP/p-induced injury by reducing LD oxidation and mitochondrial dysfunction by promoting autophagy.

4. Discussion

The present study showed that the natural small molecule Ka was a key factor by which autophagic signaling could inhibit lipid oxidative toxicity. Our results demonstrated that the autophagy pathway is a key regulatory loop through which Ka alleviates LD peroxidation and subsequent mitochondrial damage and focused on the role of autophagy-regulated LD toxicity in alleviating mitochondrial damage while preventing neurodegeneration due to excessive oxidative stress (Fig. 9).

LDs are the intracellular sites of neutral lipid storage [5]and are critical for lipid metabolism and energy homeostasis, while LD dysfunction has been linked to many diseases [16]. Accumulating evidence has suggested that the roles LDs play in biology and pathology are significantly broader than previously thought. In the CNS, evidence has shown that increased LDs in neurons and glia are implicated in neurodegenerative pathology [10,36]. In detail, LDs have been detected both in the axons of Aplysia neurons cultured in vitro [37] and in brain sections from Huntington disease models [38]. In addition, it was shown that neurons are particularly sensitive to lipid toxicity, and the accumulation of LDs that cannot be removed in a timely manner leads to accelerated LD peroxidation and can give rise to neurodegeneration [17].

Lipid accumulation in hyperactive neurons is toxic not only because of the susceptibility of these lipids to peroxidation. Moreover, the contents of the excess LDs may enter nonoxidative metabolic pathways, triggering excessive production of ceramide, which is toxic to cells [39]. Recent studies have also shown that in LD-defective cells, FAs can be converted into acylcarnitines, which then cause mitochondrial dysfunction and ROS production [40].These processes are likely to have specific and profound consequences in hyperactive neurons because dysfunctional mitochondria compromise the capacity for FA consumption, and mtROS production further causes membrane lipid peroxidation.

Thus, LD homeostasis should be well controlled in neuron, which is critical for avoiding toxicity and ultimately maintaining the health of the brain. In the present study, we have found that the small natural molecule Ka inhibits neuronal LD toxicity that manifested as increased LD accumulation, elevated lipid peroxidation, and upregulated lipid toxicity-related gene expression in MPP^+-insulted SH-SY5Y cells. More importantly, we have also shown that Ka treatment reduces the

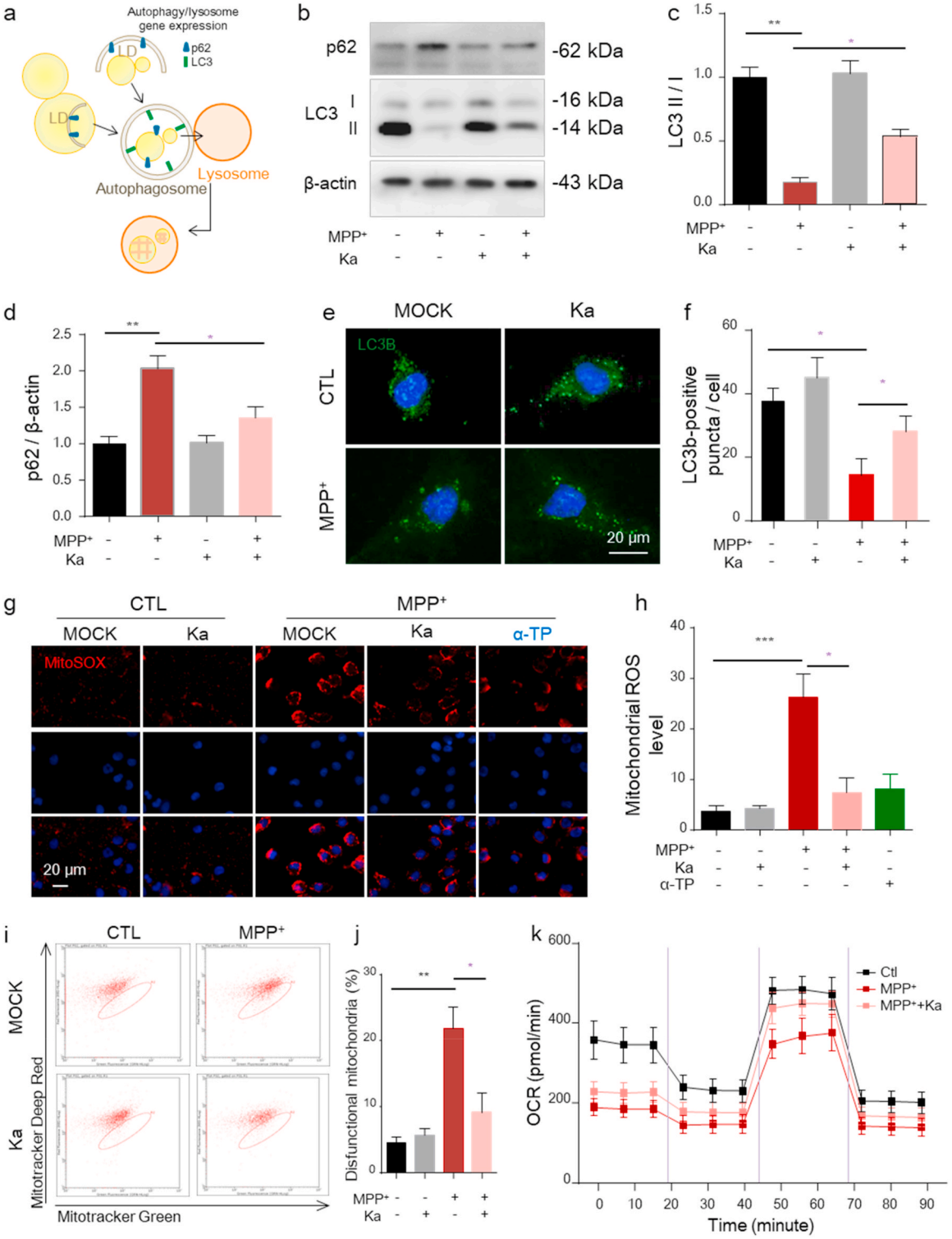

Fig. 6. Ka promotes autophagy and decreases mtROS production in MPP$^+$-treated SH-SY5Y cells.
Ka (30 μM, 3 h)-pretreated SH-SY5Y cells were stimulated with (or without) MPP$^+$ (400 μM, 24 h).(a) Degradation of LDs (LDs) via autophagy, which is known as lipophagy. (b–d) Representative immunoblots (b) and quantitative analysis of LC3 (c) and p62 (d) in the cytoplasm of SH-SY5Y cells. The quantified data are normalized to the control group.(e–f) Representative images of LC3B puncta analyzed using confocal microscopy (e). Cells were treated with bafilomycin before immunostaining. Scale bar, 20 μm. The number of LC3B puncta per cell was quantified (f). (g–h) SH-SY5Y cells were stained with MitoSOX and analyzed by confocal microscopy (g). Nuclei were stained with DAPI (blue). Scale bars, 20 μm. Quantification of MitoSOX fluorescence intensity using ImageJ software (h). (i–j) SH-SY5Y cells were stained with MitoTracker green and MitoTracker deep red and analyzed by flow cytometry (h) and the number of dysfunctional mitochondria was quantified (i). The data are expressed as the mean ± SEM of three to five independent experiments.
(k) The oxygen consumption rate (OCR) of live SH-SY5Y cells were determined by the Seahorse XF analyzer, following the injection of oligomycin, FCCP, and rotenone/antimycin A. (n = 3, mean ± SD). *$P < 0.05$, **$P < 0.01$, ***$P < 0.001$, by one-way ANOVA followed by Tukey's post hoc test. Ka, kaempferol; MPP$^+$, 1-methyl-4-phenylpyridinium. . (For interpretation of the references to colour in this figure legend, the reader is referred to the Web version of this article.)

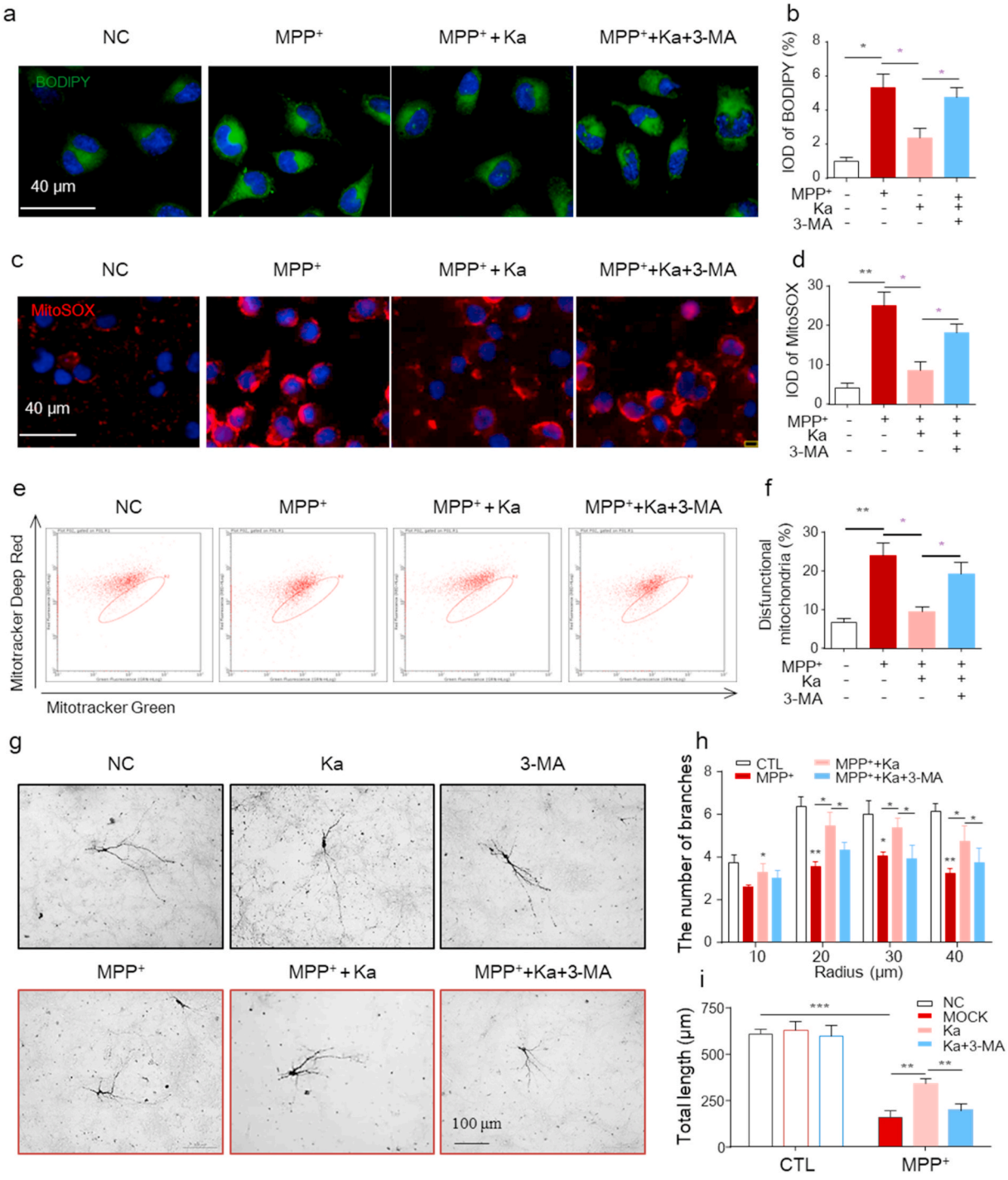

Fig. 7. Inhibiting autophagy reverses the protective effect of Ka on MPP$^+$-induced injury in neuronal cells. SH-SY5Y cells were treated with 3-MA (3 mM) for 1 h before Ka (30 μM, 3 h) treatment followed by MPP$^+$ (400 μM, 24 h) stimulation. (a–b) Representative images (a) and quantification (b) of LD accumulation in SH-SY5Y cells. Nuclei were stained with DAPI (blue). Scale bar, 40 μm. (c–d) SH-SY5Y cells were stained with MitoSOX (c), and mtROS were quantified (d). Scale bar, 40 μm. (e–f) SH-SY5Y cells were stained with MitoTracker green and MitoTracker deep red and analyzed by flow cytometry (e) and the number of dysfunctional mitochondria was quantified (f). (g–i) Mesencephalic primary neurons were pretreated with 3-MA (3 mM, 1 h), followed by Ka (30 μM, 3 h) and MPP$^+$ (50 μM, 24 h) treatment. Representative images of TH$^+$ immunostaining of neurons (g) and the quantification of the mean branch number (h) and total neurite length (i). Scale bar, 100 μm. Data are representative of three independent experiments, a total number of 17–20 neurons/treatment was quantified in (h,i). The data are expressed as the mean ± SEM of three to five independent experiments. $^*P < 0.05$, $^{**}P < 0.01$, $^{***}P < 0.001$, by one-way ANOVA followed by Tukey's post hoc test. Ka, kaempferol; MPP$^+$, 1-methyl-4-phenylpyridinium. . (For interpretation of the references to colour in this figure legend, the reader is referred to the Web version of this article.)

accumulation of LDs and decreases the expression of lipid toxicity genes in the MPTP-induced PD mouse model. These data indicate that Ka can suppress LD toxicity in vitro and in PD model mice.

Our study further reveals the molecular mechanism underlying the suppressive effects of Ka on LD-mediated toxicity. It has been demonstrated that ectopically stored LDs and the toxic lipid intermediates generated may cause deleterious effects that are collectively known as lipotoxicity and contribute to impaired cellular signaling, mitochondrial dysfunction and cell death [29,41]. Emerging evidence has revealed a negative correlation between a reduction in autophagy

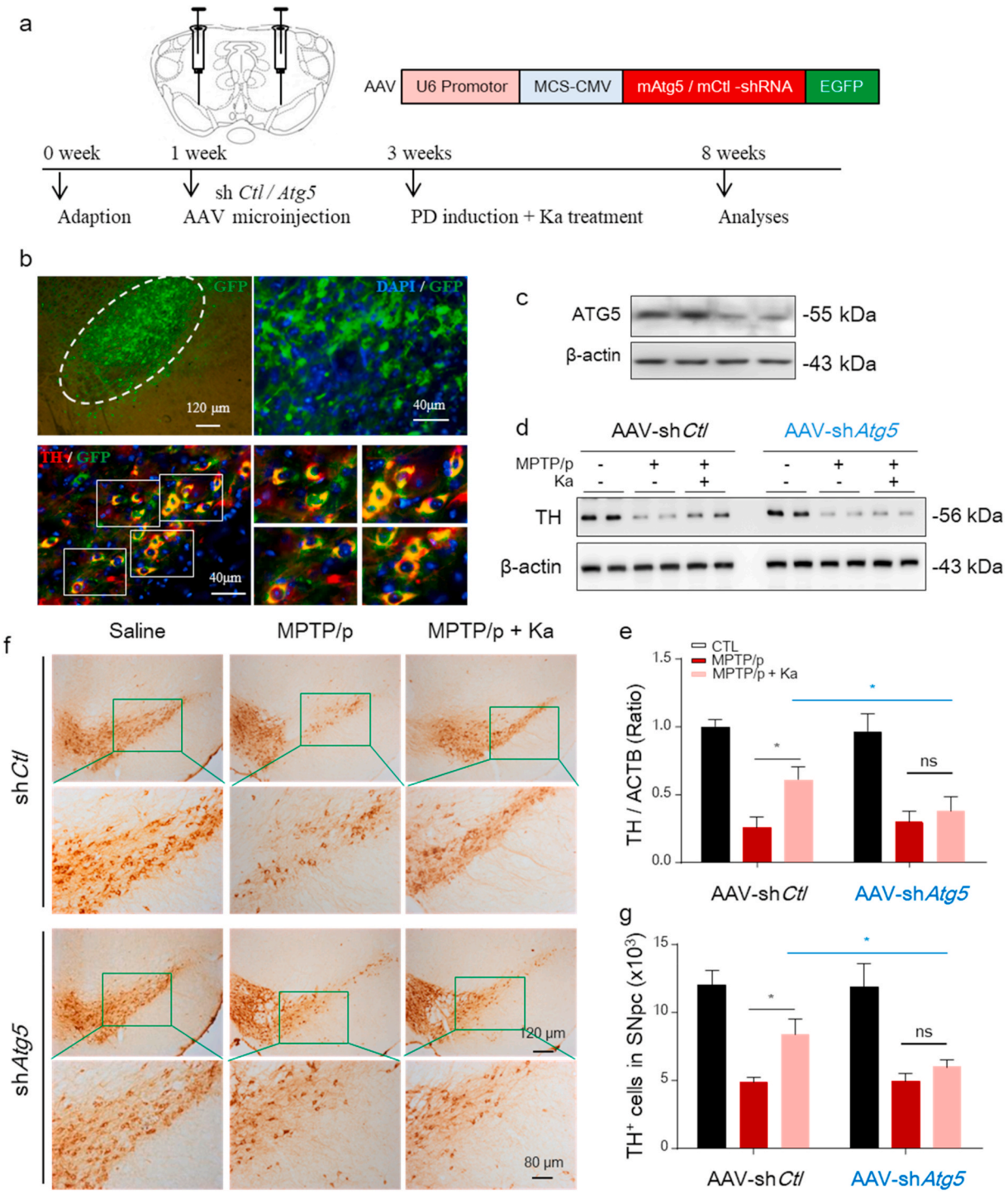

Fig. 8. *Atg5* knockdown blunts Ka-mediated inhibition of neurodegeneration in MPTP/p-injured mice.
All mice were injected with AAV-EGFP-shRNA against *Atg5* or control (1 μl of 10^{13} viral genomes/μl, bilaterally), followed by MPTP/p-induced (saline as control) injury and/or Ka treatment, as described previously. (a–b) Immunostaining verified the transfection of AAV (GFP) in TH^+ neurons (red) (a). Scale bars are as indicated. Immunoblotting confirmed the knockdown of ATG5 in the mesencephalon of injected mice (b). (c–d) Western blotting (c) and densitometric analysis (d) of TH protein levels in mesencephalon extracts of mice in the different groups. (e–f) IHC images representing TH-positive DA neurons in midbrain sections (e) and quantification (f). Scale bar is as indicated. The data are expressed as the mean ± SEM. n = 4–5 mice per group. ns, not significant, $^*P < 0.05$, $^{**}P < 0.01$, by one-way ANOVA followed by Tukey's post hoc test. Ka, kaempferol; MPTP, 1-methyl-4-phenyl-1,2,3,6-tetrahydropyridine. . (For interpretation of the references to colour in this figure legend, the reader is referred to the Web version of this article.)

and PD [42,43]. Autophagy is a catabolic degradation system by which unnecessary or damaged cellular components are degraded and recycled [44]. Evidence suggests that autophagy plays a pivotal role in maintaining cellular lipid homeostasis in multiple tissues [18,28]. Lipophagy is a recently identified, specialized form of autophagy that is involved in the removal of LDs through degradation via the autophagy-lysosomal system [18,29]. The pharmacological or genetic activation of autophagy, may delay the onset and alleviate the pathology of PD [25,44]. Lipophagy plays an essential role in PD-associated neurodegeneration, linking mitochondrial quality control to chronic neurodegeneration [38,

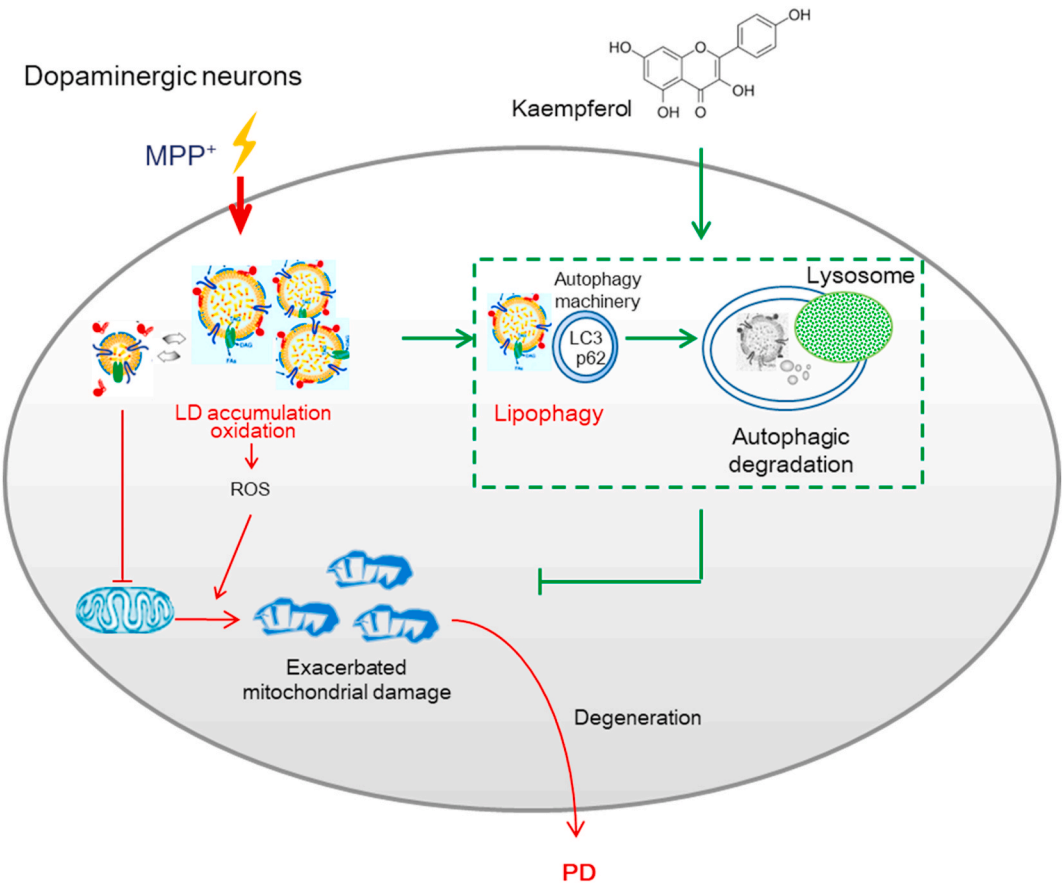

Fig. 9. Proposed model depicting Ka as an autophagy promoter to degrade accumulated LDs and prevent lipid oxidation, which alleviates mitochondrial damage and, consequently, the neurodegenerative process in Parkinson's disease.

45]. In the present study, we observed defective autophagy/lipophagy in MPP^+-injured neuronal cells, including reduced LC3-II levels and elevated p62 expression and an increased number of LC3B puncta deposited in cells. Defective lipophagy in injured SH-SY5Y cells was reversed by treatment with Ka. As a consequence, Ka decreased the accumulation of oxidized LDs, damaged mitochondria and mtROS generation in MPP^+-treated SH-SY5Y cells. Importantly, the inhibition of autophagy by 3-MA abolished the Ka-mediated elimination of oxidized LDs and damaged mitochondria and the alleviation of DA neuron injury in vitro. Moreover, the inhibition of autophagy by Atg5 knockdown in vivo reversed the protective effects of Ka on DA neuronal degeneration in the MPTP-induced PD mouse model. Collectively, these findings indicate that Ka inhibits LD toxicity-related mitochondrial damage by promoting autophagy in an experimental PD model.

Accumulating evidence indicates that increased mtROS generation is a primary characteristic of high-activity neurons and has been observed in many NDDs, including PD [46]. Reports about whether ROS are a cause or consequence of LD formation are contradictory [47,48]. Interestingly, our in vitro results demonstrated that pharmacological inhibition of LD peroxidation with α-tocopherol prevented mtROS generation and mitochondrial membrane potential abnormalities and alleviated mitochondrial reductions, as evidenced by Tomm20 staining in SH-SY5Y cells, which supports the idea that LD peroxidation plays a causal role in MPP-induced mitochondrial dysfunction and the generation of mtROS. However, it is possible that elevated ROS initially accelerate LD formation, and subsequently, LDs induce further ROS generation and exacerbate intracellular and mitochondrial ROS levels.

In the present study, we showed that mice with MPTP-induced PD had high levels of LD accumulation, which was accompanied by increased loss of DA neurons, accelerated ROS-mediated stress, and behavioral deficits. Ka treatment prevented LD toxicity in vitro and ameliorated DA neuronal loss and behavioral deficits in the PD mouse model, and these effects were autophagy-dependent. Therefore, it is reasonable to conclude that Ka promotes autophagy, and this enhanced autophagy decreases oxidized LD accumulation, reduces mtROS production, and alleviates mitochondrial damage in DA neurons, which contributes to the inhibition of LD toxicity, thereby attenuating PD pathology (Fig. 9).

Funding

This research was supported by grants from the National Natural Science Foundation of China (No. 81903587), the Project funded by China Postdoctoral Science Foundation (No. 2019M661807), the Natural Science Foundation of Jiangsu Province (No. BK20190120), and the Open Project of Chinese Materia Medica First-Class Discipline of Nanjing University of Chinese Medicine (No. 2020YLXK006), and the Drug Innovation Major Project (No. 2018ZX09711001-003-007).

Author contributions

X.H. designed and performed most of the experiments, analyzed and interpreted the data, and wrote the manuscript. S.Z. and H.S. helped performing western bolt experiment and writing the manuscript. X.T. and F.Q. performed experiments and analyzed the data. H.G. and L.S. conceived the study concept, designed the experiments.

Abbreviations:

PD Parkinson's disease

NDDs	Neurodegenerative diseases
SNpc	Substantia nigra compacta
LD	Lipid droplet;
ER	Endoplasmic reticulum
CNS	Central nervous system
FFAs	Free fatty acids
Ka	Kaempferol
MPTP	Methyl-4-phenyl-1,2,3,6-tetrahydropyridine;
i.p.	Intraperitoneally
HPLC	High Performance Liquid Chromatography
PFA	Paraformaldehyde
IHC	Immunohistochemical
BSA	Bull Serum Albumin
DAB	3,3′ -diaminobenzidine-tetrahydrochloride-dihydrate
α-TP	α-tocopherol
MPP^+	1-Methyl-4-phenylpyridinium
DA	Dopaminergic
DOPAC	Dihydroxy-phenyl aceticacid
TH	Tyrosine hydroxylase
GFAP	Glial fibrillary acidic protein
IBA-1	Ionized calcium bindingadaptor molecule-1
LDH	Lactate dehydrogenase
TEM	Transmission electron microscopy
ROS	Reactive oxygen species
LC3	Microtubule-associated protein light chain 3
NADPH	Nicotinamide adenine dinucleotide phosphate
AAV	adeno-associated virus
mtROS	Mitochondrial reactive oxygen species
DHE	Dihydroethidium
GAPDH	Glyceraldehyde-3-phosphate dehydrogenase
ANOVA	One-way analysis of variance
OCR	oxygen consumption rate

Appendix A. Supplementary data

Supplementary data to this article can be found online at https://doi.org/10.1016/j.redox.2021.101911.

Declaration of competing interest

Manuscript Number: REDOX-D-20-00757.
The authors declare no competing interests.

References

[1] W. Poewe, K. Seppi, C.M. Tanner, et al., Parkinson disease[J], Nat Rev Dis Primers 3 (2017) 17013.
[2] A. Ascherio, M.A. Schwarzschild, The epidemiology of Parkinson's disease: risk factors and prevention[J], Lancet Neurol. 15 (12) (2016) 1257–1272.
[3] T.F. Outeiro, Yeast cells provide insight into alpha-synuclein biology and pathobiology[J], Science 302 (5651) (2003) 1772–1775.
[4] Schaffer J.E. Lipotoxicity, Many roads to cell dysfunction and cell death: introduction to a thematic review series[J], JLR (J. Lipid Res.) 57 (8) (2016) 1327–1328.
[5] H.F. Hashemi, J.M. Goodman, The life cycle of lipid droplets[J], Curr. Opin. Cell Biol. 33 (2015) 119–124.
[6] M.H. den Brok, T.K. Raaijmakers, E. Collado-Camps, et al., Lipid droplets as immune modulators in myeloid cells[J], Trends Immunol. 39 (5) (2018) 380–392.
[7] B.G. Childs, D.J. Baker, T. Wijshake, et al., Senescent intimal foam cells are deleterious at all stages of atherosclerosis[J], Science 354 (6311) (2016) 472–477.
[8] O.J. Castejon, A. Castellano, G.J. Arismendi, et al., The inflammatory reaction in human traumatic oedematous cerebral cortex[J], J. Submicr. Cytol. Pathol. 37 (1) (2005) 43–52.
[9] S.C. Lee, G.R. Moore, G. Golenwsky, et al., Multiple sclerosis: a role for astroglia in active demyelination suggested by class II MHC expression and ultrastructural study[J], J. Neuropathol. Exp. Neurol. 49 (2) (1990) 122–136.
[10] L. Liu, K. Zhang, H. Sandoval, et al., Glial lipid droplets and ROS induced by mitochondrial defects promote neurodegeneration[J], Cell 160 (1–2) (2015) 177–190.
[11] M.K. Shimabukuro, L.G. Langhi, I. Cordeiro, et al., Lipid-laden cells differentially distributed in the aging brain are functionally active and correspond to distinct phenotypes[J], Sci. Rep. 6 (2016) 23795.
[12] X. Han, J. Zhu, X. Zhang, et al., Plin4-Dependent lipid droplets hamper neuronal mitophagy in the MPTP/p-Induced mouse model of Parkinson's disease[J], Front. Neurosci. 12 (2018) 397.
[13] A.S. Rambold, S. Cohen, J. Lippincott-Schwartz, Fatty acid trafficking in starved cells: regulation by lipid droplet lipolysis, autophagy, and mitochondrial fusion dynamics[J], Dev. Cell 32 (6) (2015) 678–692.
[14] P. Schönfeld, G. Reiser, Why does brain metabolism not favor burning of fatty acids to provide energy? - reflections on disadvantages of the use of free fatty acids as fuel for brain[J], J. Cerebr. Blood Flow Metabol. 33 (10) (2013) 1493–1499.
[15] K.H. Fisher-Wellman, P.D. Neufer, Linking mitochondrial bioenergetics to insulin resistance via redox biology[J], Trends Endocrinol. Metabol. 23 (3) (2012) 142–153.
[16] M.A. Welte, Expanding roles for lipid droplets[J], Curr. Biol. 25 (11) (2015) R470–R481.
[17] R. Sultana, M. Perluigi, D.A. Butterfield, Lipid peroxidation triggers neurodegeneration: a redox proteomics view into the Alzheimer disease brain[J], Free Radic. Biol. Med. 62 (2013) 157–169.
[18] Y. Zhang, S. Goldman, R. Baerga, et al., Adipose-specific deletion of autophagy-related gene 7 (atg7) in mice reveals a role in adipogenesis[J], Proc. Natl. Acad. Sci. U. S. A. 106 (47) (2009) 19860–19865.
[19] N. Martinez-Lopez, R. Singh, Autophagy and lipid droplets in the liver[J], Annu. Rev. Nutr. 35 (2015) 215–237.
[20] S.F. Nabavi, A. Sureda, A.R. Dehpour, et al., Regulation of autophagy by polyphenols: paving the road for treatment of neurodegeneration[J], Biotechnol. Adv. 36 (6) (2018) 1768–1778.
[21] C. Manach, A. Scalbert, C. Morand, et al., Polyphenols: food sources and bioavailability[J], Am. J. Clin. Nutr. 79 (5) (2004) 727–747.
[22] W.S. Da-Silva, J.W. Harney, B.W. Kim, et al., The small polyphenolic molecule kaempferol increases cellular energy expenditure and thyroid hormone activation [J], Diabetes 56 (3) (2007) 767–776.
[23] O. Morales-Ibanez, S. Affo, D. Rodrigo-Torres, et al., Kinase analysis in alcoholic hepatitis identifies p90RSK as a potential mediator of liver fibrogenesis[J], Gut 65 (5) (2016) 840–851.
[24] S.E. Park, K. Sapkota, S. Kim, et al., Kaempferol acts through mitogen-activated protein kinases and protein kinase B/AKT to elicit protection in a model of neuroinflammation in BV2 microglial cells[J], Br. J. Pharmacol. 164 (3) (2011) 1008–1025.
[25] X. Han, S. Sun, Y. Sun, et al., Small molecule-driven NLRP3 inflammation inhibition via interplay between ubiquitination and autophagy: implications for Parkinson disease[J], Autophagy 15 (11) (2019) 1860–1881.
[26] J. Zhu, Z. Hu, X. Han, et al., Dopamine D2 receptor restricts astrocytic NLRP3 inflammasome activation via enhancing the interaction of beta-arrestin2 and NLRP3[J], Cell Death Differ. 25 (11) (2018) 2037–2049.
[27] Y. Wei, M. Lu, M. Mei, et al., Pyridoxine induces glutathione synthesis via PKM2-mediated Nrf2 transactivation and confers neuroprotection[J], Nat. Commun. 11 (1) (2020).
[28] R. Singh, S. Kaushik, Y. Wang, et al., Autophagy regulates lipid metabolism[J], Nature 458 (7242) (2009) 1131–1135.
[29] B. Jaishy, E.D. Abel, Lipids, lysosomes, and autophagy[J], J. Lipid Res. 57 (9) (2016) 1619–1635.
[30] L.A. Harris, J.R. Skinner, N.E. Wolins, Imaging of neutral lipids and neutral lipid associated proteins[J], Methods Cell Biol. 116 (2013) 213–226.
[31] M.S. Ioannou, J. Jackson, S. Sheu, et al., Neuron-astrocyte metabolic coupling protects against activity-induced fatty acid toxicity[, J. Cell. 177 (6) (2019) 1522–1535.
[32] V. Jackson-Lewis, S. Przedborski, Protocol for the MPTP mouse model of Parkinson's disease[J], Nat. Protoc. 2 (1) (2007) 141–151.
[33] M.S. Parihar, T. Hemnani, Experimental excitotoxicity provokes oxidative damage in mice brain and attenuation by extract of Asparagus racemosus[J], J. Neural. Transm. 111 (1) (2004) 1–12.
[34] J. Marschallinger, T. Iram, M. Zardeneta, et al., Lipid-droplet-accumulating microglia represent a dysfunctional and proinflammatory state in the aging brain [J], Nat. Neurosci. 23 (2) (2020) 194–208.
[35] P.H. Willems, R. Rossignol, C.E. Dieteren, et al., Redox homeostasis and mitochondrial dynamics[J], Cell Metabol. 22 (2) (2015) 207–218.
[36] V. Kis, B. Barti, M. Lippai, et al., Specialized cortex glial cells accumulate lipid droplets in Drosophila melanogaster[J], PloS One 10 (7) (2015), e131250.
[37] M.J. Savage, D.J. Goldberg, S. Schacher, Absolute specificity for retrograde fast axonal transport displayed by lipid droplets originating in the axon of an identified Aplysia neuron in vitro[J], Brain Res. 406 (1–2) (1987) 215–223.
[38] M. Martinez-Vicente, Z. Talloczy, E. Wong, et al., Cargo recognition failure is responsible for inefficient autophagy in Huntington's disease[J], Nat. Neurosci. 13 (5) (2010) 567–576.
[39] R.H. Unger, G.O. Clark, P.E. Scherer, et al., Lipid homeostasis, lipotoxicity and the metabolic syndrome[J], Biochim. Biophys. Acta 1801 (3) (2010) 209–214.
[40] T.B. Nguyen, S.M. Louie, J.R. Daniele, et al., DGAT1-Dependent lipid droplet biogenesis protects mitochondrial function during starvation-induced autophagy [J], Dev. Cell 42 (1) (2017) 9–21.
[41] A.R. Wende, J.D. Symons, E.D. Abel, Mechanisms of lipotoxicity in the cardiovascular system[J], Curr. Hypertens. Rep. 14 (6) (2012) 517–531.
[42] M. Komatsu, S. Waguri, T. Chiba, et al., Loss of autophagy in the central nervous system causes neurodegeneration in mice[J], Nature 441 (7095) (2006) 880–884.
[43] W.H. Shin, J.H. Park, K.C. Chung, The central regulator p62 between ubiquitin proteasome system and autophagy and its role in the mitophagy and Parkinson's disease[J], BMB Rep 53 (1) (2020) 56–63.

[44] P. Rivero-Rios, J. Madero-Perez, B. Fernandez, et al., Targeting the autophagy/lysosomal degradation pathway in Parkinson's disease[J], Curr. Neuropharmacol. 14 (3) (2016) 238–249.
[45] L. Liu, K. Zhang, H. Sandoval, et al., Glial lipid droplets and ROS induced by mitochondrial defects promote neurodegeneration[J], Cell 160 (1–2) (2015) 177–190.
[46] L.F. Burbulla, P. Song, J.R. Mazzulli, et al., Dopamine oxidation mediates mitochondrial and lysosomal dysfunction in Parkinson's disease[J], Science 357 (6357) (2017) 1255–1261.
[47] T. Inoguchi, P. Li, F. Umeda, et al., High glucose level and free fatty acid stimulate reactive oxygen species production through protein kinase C–dependent activation of NAD(P)H oxidase in cultured vascular cells[J], Diabetes 49 (11) (2000) 1939–1945.
[48] S.J. Lee, J. Zhang, A.M. Choi, et al., Mitochondrial dysfunction induces formation of lipid droplets as a generalized response to stress[J], Oxid Med Cell Longev 2013 (2013) 327167.